Numerical Heat Transfer-Part A (USA)

https://www.tandfonline.com/toc/unht20/current

Accepted February 3rd, 2024.

Computational analysis of magnetized Casson liquid stretching flow adjacent to a porous medium with Joule heating, stratification, multiple slip and chemical reaction aspects

M. Nasir[1], M. S. Kausar[2], M. Waqas[3], O. Anwar Beg[4], S. S. Abdullaev[5,6], Salah Saadaoui[7] and W. A. Khan[8]*

[1,2]Faculty of Informatics and Computing, University Sultan Zainal Abidin, Kuala Terengganu, Terengganu 21300, Malaysia

[3]NUTECH School of Applied Science and Humanities, National University of Technology, Islamabad 44000, Pakistan

[4]Professor and Director-Multi-Physical Engineering Sciences Group, Mechanical Engineering, Salford University, School of Science, Engineering and Environment (SEE), Manchester, M54WT, UK

[5]Researcher, Faculty of Chemical Engineering, New Uzbekistan University, Tashkent, Uzbekistan

[6]Researcher of Scientific Department, Tashkent State Pedagogical University named after Nizami, Tashkent, Uzbekistan

[7]Department of Physics, Faculty of Science and Arts, Mohayel Aser, King Khalid University, Abha, Saudi Arabia

[8]Department of Mathematics, Mohi-ud-Din Islamic University, Nerian Sharif, Azad Jammu & Kashmir, 12010, Pakistan

**Correspondence*: mw_qau88@yahoo.com

ABSTRACT: This article aims to investigate the characteristics of thermo-solutal magnetohydrodynamic (MHD) non-Newtonian smart coating boundary layer flow of a stretching substrate adjacent to a porous medium, considering the influence of chemical reactions and thermal radiation subject to a transverse static magnetic field. A non-Darcy drag force model is deployed to capture both Darcy bulk drag and inertial Forchheimer (quadratic) drag effects. A diffusion flux model is deployed for radiative heat transfer. The Casson viscoplastic model has been utilized to simulate rheological characteristics. Due to polymeric slip effects, three slip phenomena are included at the wall (hydrodynamic, thermal and concentration) in the formulation. Furthermore, viscous dissipation and Ohmic heating (Joule dissipation) are also included. Robust scaling similarity variables are deployed to transform the governing partial differential equations into ordinary differential equations. Subsequently, the emerging dimensionless coupled nonlinear boundary value problem is solved utilizing the Bvp4c method in MATLAB version 2022. This numerical approach allows for a logical parametric examination of all key control parameters on the transport phenomena, enabling a comprehensive understanding of the system behavior. Validation with previous studies is included. Detailed graphical and tabular computations are included for velocity, temperature, concentration, skin friction, Nusselt number and Sherwood number, for the influence of Darcian parameter, Forchheimer inertial parameter, mixed convection, velocity (momentum) slip, magnetic number, Casson parameter, nonlinear thermal convection parameter, nonlinear concentration convection parameter, radiation parameter, thermal stratification parameter, Prandtl number, heat source/sink parameter, Eckert number, thermal slip parameter, Schmidt number, chemical reaction, solutal stratification parameter and solutal slip parameter. Detailed interpretation of the physics associated with these multiple effects is included. Flow deceleration is observed with increment in Darcy parameter, Forchheimer parameter, Hartmann number, Casson parameter and momentum slip whereas flow acceleration is computed with increasing mixed convection parameter. Temperatures are accentuated with elevation in Rosseland radiative parameter, magnetic parameter, thermal stratification parameter, heat source parameter and Eckert (dissipation) number, whereas it is depleted with thermal slip (jump) parameter, heat sink, Prandtl number and mixed convection parameter. An increment in Schmidt number, first order homogenous chemical reaction parameter, solutal stratification parameter and mass slip parameters induce a reduction in concentration magnitudes and species boundary layer thickness. Skin friction is elevated with Darcian parameter. Nusselt number is boosted with mixed convection parameter whereas it is suppressed with radiation parameter, magnetic number, Casson parameter, thermal stratification parameter and thermal slip parameter. Sherwood number is observed to decay with increment in solutal stratification parameter and solutal slip parameter whereas it is enhanced with Schmidt number and chemical reaction parameters. The simulations provide further insight into the transport characteristics of electromagnetic viscoplastic coating material manufacturing.

KEYWORDS: *MHD, thermal radiation, chemical reaction, Casson viscoplastic fluid, heat generation and heat absorption, slips boundary conditions, Bvp4c method; MATLAB; smart magnetic polymers.*

NOMENCLATURE

Roman

B_o	Magnetic field strength ($Nm^{-1}A^{-1}$);
C_f	Skin friction coefficient;
C_∞	Ambient solute concentration (moles/m^3);
Ec	Eckert number;
f	Dimensionless stream function;
Gr_x	Thermal buoyancy number;
Gr_x^*	Concentration buoyancy number;
M	Magnetic interaction number;
N	Buoyancy ratio parameter
Nu_x	Local Nusselt number;
Pr	Prandtl number;
R	Rosseland radiation parameter;
Re_x	Local Reynolds number;
S	Heat source/sink parameter;
Sc	Schmidt number
S_1	Velocity (hydrodynamic) slip parameter;
S_2	Thermal slip (jump) parameter;
S_3	Solutal (mass) slip parameter;
T	Fluid temperature (K);
T_∞	Ambient fluid temperature (K);
u, v	velocity components (ms^{-1});
x, y	coordinate axes (m)

Greek

α_1	Darcian parameter;
α_2	Forchheimer inertial parameter;
β	Casson non-Newtonian parameter;
β_t	nonlinear thermal convection parameter;
β_c	nonlinear concentration convection parameter;
θ	Dimensionless temperature;
ρ	Density of base-fluid (kgm^{-3});
ε_1	thermal stratification parameter;

ε_2 Solutal stratification parameter;
η Similarity variable;
Φ porosity of porous medium;
λ mixed convection parameter;

1.INTRODUCTION

The study of non-Newtonian fluids is important in a range of real-world applications including polymer processing, plastics, injection molding, shrink-fit wrapping and complex sensor coatings. An extensive body of literature has therefore emerged focusing on simulations of various non-Newtonian fluids in manufacturing processes involving these technologies. Non-Newtonian fluids are characterized by nonlinear relationships between the rate of strain and the shear stress. This leads to exceedingly complex and nonlinear convoluted differential equations in mathematical models. Numerous different formulations have been developed largely in the 20th century to address the many complex features of such liquids (which include polymers, lubricants, food stuffs, slurries) such as pseudoplasticity, dilatancy, viscoelasticity, thixotropy, fading memory, stress relaxation and retardation and yield stress behaviour [1,2]. Another important category of non-Newtonian fluids is magnetic polymers which combined electroconductive properties with polymer rheology [3]. These magnetic composites have excellent abilities for being synthesized into complicated shapes for use in for example sensors and actuators in automation equipment and medical devices. Popular techniques for their fabrication include compression molding, injection molding, calendaring and sheet extrusion. External magnetic fields can be used to manipulate the functionalities of these complex fluids, and this requires magnetohydrodynamic (MHD) simulations. In many of these manufacturing processes, high temperature arises, and radiative heat transfer is also significant [4-6]. Important models developed for simulating magnetic polymer flows include the Reynolds variable viscosity model [7], tangent hyperbolic model [8], Maxwell upper convected (UCM) viscoelastic model [9, 10], Eringen micropolar model [11], Cross model [12] and Jeffrey viscoelastic model [13], PPT viscoelastic model, Carreau shear-thinning model, Herschel-Bulkley combined power-law and yield stress model etc. The viscoplastic Casson model has proved especially popular for certain electroconductive polymers (ECPs). This non-Newtonian model features shear thinning and thickening in addition to yield stress characteristics. Casson fluids demonstrate both fluid and solid-like behaviors depending on the circumstances. The Casson fluid assumes a solid state if shear stress experienced is beneath the threshold value of yield stress. The Casson fluid has been applied to many complex industrial and geophysical fluids including food stuffs, confectionery, thermoplastics, magnetic biopolymers, biological fluids (blood), pigments, coal slurries, artificial solvents, China clay, muddy sediments. There is a high degree of thermal transport in Casson fluids as compared to Newtonian fluids. The Casson model was introduced by Casson [14] to simulate rheological properties of suspensions of pigment oil. It has ben implemented in many studies primarily due to its popularity in manufacturing processes and also medicine. These studies have also included a number of other multi-physical phenomena including magnetohydrodynamics (MHD), heat absorption/generation, complex boundaries, conductive, convective and radiative heat transfer, porous media etc. Alhadhrami *et al.* [15] examined Casson fluid behaviour in laminar non-equilibrium flow in porous media using a Runge-Kutta- 4^{th} order shooting method. Akhtar *et al.* [16] presented closed-form solutions for peristaltic pumping and thermo-solutal transport in Casson fluid through an elliptic conduit, noting that strong flow acceleration arises in the core. Samrat *et al.* [17] studied the relative performance of Casson, Williamson and Carreau fluids in boundary layer convective flow from a stretching semi-parabolic geometry with exponential heat generation using MATLAB bvp4c quadrature. They observed that Casson fluid achieves superior thermal conductivity when compared to Carreau and Williamson fluids and also that Nusselt number is boosted with increasing exponential heat source effects. Many other studies have been communicated on industrial flows of magnetic Casson fluids including Akbar *et al.* [18] (on bio-inspired pumping of magnetized Casson fluids), Awais *et al.* [19] (on double diffusive MHD Casson flow from a contracting wall), Vasu *et al.* [20] (on micro-organism doped electroconductive Casson thin film deposition), Prakash *et al*. [21] (on rotating coating deposition of Casson hybrid nanofluids under dual electrical and magnetic fields) and Shahidi *et al.* [22] (on thermal relaxation effects in radiative-convective magnetic Casson polymer extrusion flow).

The above studies have generally neglected viscous and Joule heating (Ohmic dissipation). Both these phenomena are known to arise in real magnetic polymer flows and can substantially modify momentum and heat transport characteristics. Viscous heating is associated with internal friction of the fluid. Joule heating is associated with kinetic energy lost due to action of the magnetic field. Several investigations have been conducted to examine the collective effects of Joule and viscous dissipation in magnetohydrodynamic manufacturing flows. Zueo *et al.* [20] employed a network electro-thermal PSPICE code to compute the study particle deposition in magnetic coating flow. They showed that thermal boundary layer thickness is reduced with greater viscous heating and Joule dissipation effects and that flow deceleration is also induced. Kausar *et al.* [24] examined the radiative-radiative micropolar Hiemenz flow with dissipation effects, observing that wall couple stress is also modified with Eckert (dissipation) number. Thumma *et al.* [25] considered the combined Ohmic and viscous heating effects on magnetized Buongiorno nanofluid from an extending or contracting tilted boundary. Further investigations include Awais *et al.* [26, 27] (on bioconvective nanofluid flow from a stretching surface and swirling hydromagnetic flow), Kumar *et al.* [28] (on time-dependent polar couple stress hydromagnetic boundary layers), Kausar *et al*. [29] (on micropolar nanofluids with wall transpiration), Shamshuddin *et al.* [30] (on Chebyshev collocation computation of radiative Maxwell viscoelastic alumina-titania nanofluid double-diffusive convection) transport from a stretching sheet with Joule heating.

An important aspect of modern manufacturing processing is the control of chemical reactions. Cheaper raw materials can be produced in order to create high-quality products with suitable chemical reaction. In this case, fluid dynamics plays one of the most crucial roles in terms of establishing an effective final product. A chemical reaction can be homogeneous or heterogeneous, depending on the type of chemical reaction. A homogeneous reaction occurs when the reactants and the output products are of the same physical state, but a heterogeneous reaction involves multiple phases and consists of different reactants and products. Chemical reactions are not orderly in the sense that the rate at which each reactant is concentrated depends on the power of the reaction. Thus, in first-order reactions, there is only one species and in n^{th}-order reactions n species are involved in the complete process. Reactive flows in Casson fluids are of considerable interest to reaction process engineering in polymers and have received considerable attention. Relevant studies include Murugan *et al.* [31] who studied the influence of both electrical and magnetic fields on hydrodynamic dispersion in multi-stage chemical reactions in pulsatile transport in thermal ducts. Shamshuddin *et al.* [32] computed the influence of homogeneous–heterogeneous reactions on magnetohydrodynamic non-Newtonian (Sisko) fluid from a bi-directional stretching sheet in a permeable medium. They showed that increasing homogenous chemical reaction parameter mildly decreases concentration magnitude whereas stronger heterogeneous chemical reaction parameter induces a significant depletion. Garvandha *et al.* [33] computed the phase change with second order chemical reactions in enrobing magnetic nanopolymer flow on an inclined stretching cylinder. Reddy *et al.* [34] analyzed the chemical reaction effects on both Williamson and Casson fluids from a stretching surface, noting that the flow is more strongly accelerated for Casson fluid whereas higher temperature and concentration are computed for the Williamson fluid. Shah *et al.* [35] computed the collective effects of chemical reaction and bio-convection on hydromagnetic hybrid nanofluid flow. Sudarsana *et al.* [36] simulated the radiative flux and chemical reaction effects on dual stratified double-diffusive nanofluid convection. Further investigations have been communicated by Yousef *et al.* [37] (for dissipative Casson-Williamson nanofluids) and Nasir *et al.* [38] (for Oldroyd-B nanofluids with mixed convective boundary conditions)

Another significant fluid dynamic phenomenon arising in industrial polymeric manufacturing is the presence of *wall slip*. This features in for example extrusion processes and conveyor belts and arises due to molecular dynamics at the boundary between the fluid and the substrate. It manifests as non-adherence of coatings to the substrate. Lou et al. [39] have confirmed experimentally the significant influence of hydrodynamic slip on the polymer wall behavior, using micro-injection experiments. They have shown that in particular when the wall is hydrophobic, the polymer liquid (melt) exhibits significant wall slip. With an increase in external body forces e. g. pressure, magnetic field, electrical field etc, molecular chains gradually start to separate, such that the single molecular chain becomes untangled from the entangled grid, and the chain detaches from the wall after exceeding a certain threshold. As a result, the wall slip reduces the interface thermal resistance between the solid–liquid interface and enhances the interface heat transfer performance. Many other excellent studies have confirmed these findings including Dawson *et al.* [40], Liu and Gehde [41] and Ge and Chen [42] (who deployed molecular dynamics simulations). In coating extrusion, these effects can significantly influence the characteristics of heat, mass, and momentum. To evaluate more precisely the impact of slip effects on transport characteristics of fabricated materials, a number of complex boundary value problems have been examined in recent years. These have also featured different types of wall slip including momentum (hydrodynamic) slip, thermal and mass jump (slip) effects. Faisal *et al.* [43] computed the time-dependent bioconvective nanofluid axisymmetric boundary layer flow on a stretching cylinder with momentum, thermal, solute (mass) and also micro-organism slip effects. Zubair *et al.* [44] analyzed the combined effects of thermal and momentum slip on magnetized stretching sheet flow with radiative flux. Shamshuddin *et al.* [45] computed the influence of nonlinear hydrodynamic and thermal wall slip on three-dimensional extrusion flow of a magnetic polymer with viscous and Ohmic dissipation effects. Subba Rao *et al.* [46] used Keller's box finite difference method to compute the stagnation flow on a spherical body immersed in Casson viscoplastic fluid with velocity and thermal slip. Many other studies have been communicated for multiple slip effects in polymeric fluid boundary layer and other configurations including Khan *et al*. [47] (Oldroyd-B nanofluids), Javid *et al.* [48] (Jeffrey viscoelastic fluids), Wang *et al.* [49] (Maxwell fluids), Raza *et al.* [50] (radiative heat transfer), Rana and Gupta [51] (thermo-capillary convection from a disk), Madhukesh *et al.* [52] (non-Fourier hydromagnetic micropolar-Casson nanofluids), Krishna *et al.* [53 (rotating flows of ionized Newtonian fluids with Hall current and thermo-diffusion effects), Kausar *et al.* [54] (Non-Darcy dissipative porous medium flows), Zainal *et al.* [55] (stagnation point nanofluid flows), Uddin *et al.* [57] (magnetized couple stress nanofluids), Sajid *et al.* [58] (rotating two-phase Prandtl nanofluids with radiative flux), Mahmoud et al. [59] (radiative magneto-micropolar fluids) and Uddin *et al*. [60] (Falkner-Skan magnetized micro-organism doped nanofluids with electromagnetic induction). All these studies confirmed that significant modifications in all transport characteristics especially at the wall are induced with slip effects.

A scrutiny of the literature has identified that to date no mathematical study has been reported on the *thermo-solutal magnetohydrodynamic (MHD) dissipative non-Newtonian Casson viscoplastic coating boundary layer flow of a stretching substrate adjacent to a porous medium, considering the influence of chemical reactions and thermal radiation subject to a transverse static magnetic field*. *This is the novelty and focus of the present article which motivated by magnetic polymer manufacturing applications, explores the combined effects of Darcy and Forchheimer drag forces, radiative flux (via the Rosseland model), hydrodynamic, thermal and concentration slip, heat source/sink [59, 60] and dual thermal/solutal stratification effects [61-63] on transport characteristics. Additionally viscous dissipation and Ohmic heating (Joule dissipation) are included*. Robust scaling similarity variables are deployed to transform the governing partial differential equations into ordinary differential equations. Subsequently, the emerging dimensionless coupled nonlinear boundary value problem is solved utilizing the Bvp4c method in MATLAB version 2022 [64]. This numerical approach allows for a logical parametric examination of all key control parameters on the transport phenomena, enabling a comprehensive understanding of the system behavior. Validation with previous studies is included. Detailed graphical and tabular computations are included for velocity, temperature, concentration, skin friction, Nusselt number and Sherwood number, for the influence of Darcian parameter, Forchheimer inertial parameter, mixed convection, velocity (momentum) slip, magnetic number, Casson parameter, nonlinear thermal convection parameter, nonlinear concentration convection parameter, radiation parameter, thermal stratification parameter, Prandtl number, heat source/sink parameter, Eckert number, thermal slip parameter, Schmidt number, chemical reaction, solutal stratification parameter and solutal slip parameter. Extensive interpretation is provided. The computations provide a deeper insight into the fluid dynamics associated with electro-conductive viscoplastic polymer manufacture.

2.MATHEMATICAL MODEL

As a simulation of smart magnetic polymeric coating processes, the hydromagnetic viscoplastic (Casson) convective-radiative boundary layer flow from a two-dimensional stretching surface to a dual stratified non-Darcy porous medium is considered. The flow is steady, laminar and incompressible. It is presumed that the stretching velocity of the porous sheet is $U_w(x) = cx$ for $c > 0$. A Cartesian coordinate system (*x, y*) is taken to describe the flow behavior, where *x and y* are the coordinates along the surface and normal to it, respectively. A uniform transverse magnetic field of strength B_0 is applied parallel to the $y-$ axis. and the induced magnetic field is assumed to be negligible. Heat transfer from the sheet to the fluid is proportional to the local surface temperature T. The polymer is optically thick and absorbs and reflects but does not scatter thermal radiation. Rosseland's diffusion flux algebraic model is deployed. The physical model is depicted in **Fig. 1**.

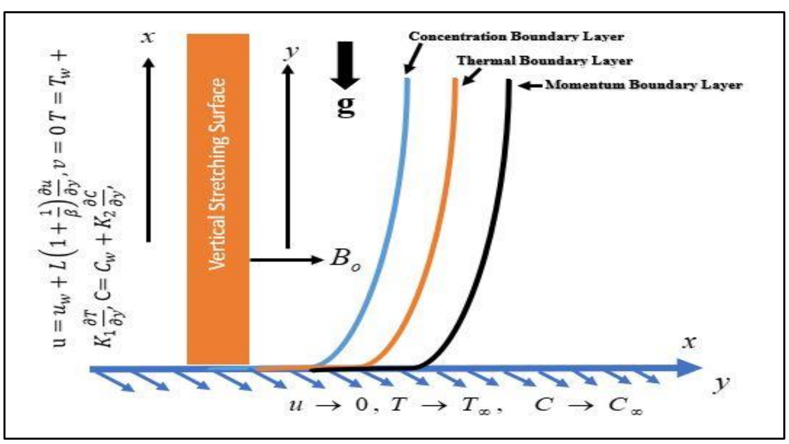

Fig. 1. Physical model.

We assume that the rheological equation for an isotropic and incompressible Casson fluid is following [1, 14]:

$$\tau = \tau_o + \mu\dot{\sigma}, \tag{1}$$

i.e.

$$\begin{aligned}\tau_{ij} &= \left\{ 2\left(\mu_B + \frac{p_y}{\sqrt{2\pi}} \right) e_{ij}, \pi > \pi_c \right\} \\ &= \left\{ 2\left(\mu_B + \frac{p_y}{\sqrt{2\pi_c}} \right) e_{ij}, \pi_c < \pi \right\},\end{aligned} \tag{2}$$

Here τ is the shear stress, τ_0 is the Casson yield stress, μ is the dynamic viscosity, $\dot{\sigma}$ is the shear rate, $\pi = e_{ij}.e_{ij}$ and e_{ij} is the (i, j)th element of the distortion rate, π is the product of the component of deformation rate with itself, π_c is a critical value of this product based on the non-Newtonian model, μ_B the is plastic dynamic viscosity of the non-Newtonian fluid and p_y is the yield stress of the fluid. Under the aforesaid assumptions, the boundary layer equations governing the flow can be written as follows:

$$\frac{\partial u}{\partial x} + \frac{\partial v}{\partial y} = 0, \tag{3}$$

$$\begin{aligned}u\frac{\partial u}{\partial x} + v\frac{\partial u}{\partial y} &= \nu\left(1+\frac{1}{\beta}\right)\frac{\partial^2 u}{\partial y^2} - \frac{\sigma B_0^2}{\rho}u - \frac{\nu\Phi}{K^*}u\left(1+\frac{1}{\beta}\right) - \frac{C_b^*\Phi}{\sqrt{K^*}}u^2 \\ &+g\left\{\Lambda_1\left(T-T_\infty\right)+\Lambda_2\left(T-T_\infty\right)^2\right\} + g\left\{\Lambda_3\left(C-C_\infty\right)+\Lambda_4\left(C-C_\infty\right)^2\right\},\end{aligned} \tag{4}$$

$$u\frac{\partial T}{\partial x} + v\frac{\partial T}{\partial y} = \alpha\frac{\partial^2 T}{\partial y^2} + \frac{16\sigma^* T_\infty^3}{3k^*\rho c_p}\frac{\partial^2 T}{\partial y^2} + \frac{Q_0}{\rho c_p}\left(T-T_\infty\right) + \frac{\sigma B_0^2}{\rho c_p}u^2 + \frac{\mu}{\rho c_p}\left(1+\frac{1}{\beta}\right)\left(\frac{\partial u}{\partial y}\right)^2, \tag{5}$$

$$u\frac{\partial C}{\partial x} + \upsilon\frac{\partial C}{\partial y} = D\frac{\partial^2 C}{\partial y^2} - k_1\left(C-C_\infty\right), \tag{6}$$

$$\begin{aligned}&u = U_w(x) + L\left(1+\frac{1}{\beta}\right)\frac{\partial u}{\partial y}, v = 0, T = T_w(x) + K_1\frac{\partial T}{\partial y}, \\ &C = C_w(x) + K_2\frac{\partial C}{\partial y} \text{ at } y = 0.\end{aligned} \tag{7}$$

$$\begin{aligned}&u \to 0, T \to T_\infty = T_0 + a_1 x, C \to C_\infty = C_0 + a_2 x, \\ &U_w(x) = cx, T_w(x) = T_0 + a_3 x, C_w(x) = C_0 + a_4 x \text{ as } y \to \infty.\end{aligned} \tag{8}$$

Here $\nu\left(=\frac{\mu}{\rho}\right)$ represents the kinematic viscosity, ρ fluid density, μ dynamic viscosity , Q_0 heat absorption/generation coefficient, k the thermal conductivity, Φ porosity of porous medium, K^* the permeability, *(a1,a2)* are dimensional constants, C liquid concentration**,** Λ_1 thermal expansion coefficient, K_1 the thermal slip variable, (β_T, β_C) the thermal/concentration expansion coefficients, $\alpha=\frac{k}{\rho c_p}$ the thermal diffusivity, σ the electrical conductivity of the magnetic polymer, T liquid temperature, L the velocity slip variable, $u_w(x)$ the stretching velocity, Λ_2 for concentration expansion coefficient, σ^* the Stefan-Boltzmann constant, g gravitational acceleration, B_o the strength of magnetic field, C_∞**,** k^* the mean absorption coefficient, C_b^* the drag coefficient, k_1 reaction rate, T_∞ temperature ambient liquid**,** β the material variable (Casson fluid), K_2 the solutal slip variable, c is a dimensional constant, $\boldsymbol{u}, \boldsymbol{v}$ are the components of velocity in the (x, y) directions respectively. Introducing the similarity transformations:

$$\begin{cases} \eta = y\sqrt{\frac{c}{\upsilon}}, u = cxf'(\eta), v = -\sqrt{c\upsilon}\, f(\eta), \\ \theta(\eta) = \frac{T - T_\infty}{T_w - T_0}, \phi(\eta) = \frac{C - C_\infty}{C_w - C_0}. \end{cases} \tag{9}$$

Eq. (1) is gratified automatically. Eqns. (4-8) yield:

$$\left(1+\frac{1}{\beta}\right)f''' + ff'' - f'^2 - M^2 f' - \alpha_1\left(1+\frac{1}{\beta}\right)f' - \alpha_2 f'^2 + \lambda\left[(1+\beta_t\theta)\theta + N(1+\beta_c\phi)\phi\right] = 0, \tag{10}$$

$$\left(1+\frac{4}{3}R\right)\theta'' + \Pr f\theta' - \Pr f'\theta - \Pr\varepsilon_1 f' + \Pr S\theta + \Pr EcM^2 f'^2 + \Pr Ec\left(1+\frac{1}{\beta}\right)f''^2 = 0, \tag{11}$$

$$\phi'' + Scf\phi' - Scf'\phi - Sc\varepsilon_2 f' - Sc\gamma\phi = 0, \tag{12}$$

$$\begin{gathered} \boldsymbol{f(0) = 0, f'(0) = 1 + S_1\left(1+\frac{1}{\beta}\right)f''(0),} \\ \boldsymbol{\theta(0) = 1 - \epsilon_1 + S_2\theta'(0), \phi(0) = 1 - \epsilon_2 + S_3\phi'(0),} \end{gathered} \tag{13}$$

$$f' \to 0, \theta \to 0, \phi \to 0 \text{ as } \eta \to \infty. \tag{14}$$

Here $(')$ signifies differentiation concerning η, β nonlinear Casson parameter, M is magnetic interaction number, λ is the mixed convection parameter, Gr_x the thermal buoyancy number, Gr_x^* the concentration buoyancy number, N the buoyancy ratio parameter, β_t is the nonlinear thermal convection parameter, Sc the Schmidt number, Pr the Prandtl number, $(S > 0)$ for heat source and heat sink $(S < 0)$, β_c nonlinear concentration convection parameter, ε_1 the thermal stratification parameter, Ec for Eckert number, ε_2 solutal stratification parameter, R is the Rosseland radiation parameter, γ the chemical reaction parameter, α_1 porosity parameter, α_2 the inertia coefficient parameter, S_1 velocity slip parameter, S_2 thermal slip parameter, S_3 solutal slip parameter. These parameters are defined as follows:

$$\begin{gathered}
M=\frac{\sigma\beta^2{}_0}{\rho c},\lambda=\frac{Gr_x}{\mathrm{Re}^2},Gr_x=\frac{g\Lambda_1\left(T_f-T_\infty\right)x^3}{\nu^2},\mathrm{Re}_x=\frac{xu_w}{\upsilon},\beta_t=\frac{\Lambda_2\left(T_f-T_\infty\right)}{\Lambda_1},, \\
N=\frac{Gr_x^*}{Gr_x},Gr_x^*=\frac{g\Lambda_3\left(C_f-C_\infty\right)x^3}{\nu^2},Sc=\frac{\upsilon}{D},\mathrm{Pr}=\frac{\upsilon}{\alpha},\beta_c=\frac{\Lambda_4 C_\infty}{\Lambda_3}, \\
S=\frac{Q_0}{\rho c_p c},R=\frac{4\sigma^* T_\infty^3}{kk^*},\varepsilon_1=\frac{\alpha_1}{\alpha_3},\varepsilon_2=\frac{\alpha_2}{\alpha_4},\gamma=\left(\frac{k_1}{c}\right),S_1=L\left(\frac{c}{\upsilon}\right)^{\frac{1}{2}} \\
\alpha_1=\frac{\nu\Phi}{cK^*},\alpha_2=\frac{C_b^*\Phi}{\sqrt{K^*}},S_2=K_1\left(\frac{c}{\upsilon}\right)^{\frac{1}{2}},S_2=K_2\left(\frac{c}{\upsilon}\right)^{\frac{1}{2}},Ec=\frac{u^2{}_w}{c_p\left(T_w-T_0\right)}.
\end{gathered} \tag{15}$$

Wall skin friction $\left(C_{f_x}\right)$ along with the local Nusselt and Sherwood numbers i. e. wall heat transfer rate and wall mass transfer rate, (Nu_x, Sh_x) take the following mathematical forms:

$$C_{f_\infty}=\frac{\tau_w}{\rho_f U_w^2},\tau_w=\left[\mu\left(1+\frac{1}{\beta}\right)\left(\frac{\partial u}{\partial y}\right)\right]_{y=0}, \tag{16}$$

$$Nu_x=\frac{xq_w}{k\left(T_w-T_0\right)},q_w=-k\left(\frac{\partial T}{\partial y}\right)_{y=0}-\frac{16\sigma^* T_\infty^3}{3k^*}\left(\frac{\partial T}{\partial y}\right)_{y=0}, \tag{17}$$

$$Sh_x=\frac{xq_m}{D\left(C_w-C_0\right)},q_m=-D\left(\frac{\partial C}{\partial y}\right)_{y=0}. \tag{18}$$

$$C_{f_x}\mathrm{Re}_x^{\frac{1}{2}}=\left(1+\frac{1}{\beta}\right)f''(0), \tag{19}$$

$$Nu_x\mathrm{Re}_x^{\frac{1}{2}}=-\left(1+\frac{4}{3}R\right)\theta'(0), \tag{20}$$

$$Sh_x\mathrm{Re}_x^{-\frac{1}{2}}=-\phi'(0), \tag{21}$$

3.NUMERICAL SOLUTION METHODOLOGY

The nonlinear boundary value problem (10)-(12) subject to the corresponding boundary conditions (13)-(14) has been solved computationally with the Bvp4c built-in quadrature function in MATLAB (version 22) symbolic software version [64, 65]. For the solutions, the following substitutions are deployed:

$$f = y_1, f' = y_2, f'' = y_3, f''' = yy_1, \tag{22}$$

$$\theta = y_4, \theta' = y_5, \theta'' = yy_2, \tag{23}$$

$$\phi = y_6, \phi' = y_7, \phi'' = yy_3, \tag{24}$$

The resulting first-order ordinary differential equations are then produced:

$$yy_1 = \left(\frac{1}{\left(1+\frac{1}{\beta}\right)}\right)\left[y^2{}_2 - y_1y_3 + M^2y_2 + \alpha_1\left(1+\frac{1}{\beta}\right)y_2 + \alpha_2 y^2{}_2 - \lambda\left[(1+\beta_t y_4)y_4 + N(1+\beta_c y_6)y_6\right]\right], \tag{25}$$

$$yy_2 = \left(\frac{1}{\left(1+\frac{4}{3}R\right)}\right)\left[\Pr y_2y_4 - \Pr y_1y_5 + \Pr \varepsilon_1 y_2 - \Pr Sy_4 - \Pr EcM^2y^2{}_2 - \Pr Ec\left(1+\frac{1}{\beta}\right)y_3{}^2\right], \tag{26}$$

$$yy_3 = Scy_2y_6 - Scy_1y_7 + Sc\varepsilon_2 y_2 + Sc\gamma y_6. \tag{27}$$

Boundary conditions for the above first-order differential systems are:

$$y_1(0) = 0,\ \ y_2(0) = 1 + S_1\left(1+\frac{1}{\beta}\right)y_3(0),\ y_4(0) = 1 - \varepsilon_1 + S_2y_5(0),\ y_6(0) = 1 - \varepsilon_2 + S_3y_7(0)\ . \tag{28}$$

$$y_2(\infty) = 0,\ \ y_4(\infty) = 0,\ \ y_6(\infty) = 0\ . \tag{29}$$

4.VALIDATION OF BVP4C

To verify the accuracy of the MATLAB Bvp4c computations, comparisons have been made with earlier simpler models computed by Yousef *et al.* [37] and Mahmoud [58] for skin friction in the Newtonian case in the absence of porous media, magnetic, mixed convection and momentum wall slip effects. **Table 1** shows the comparison and clearly excellent correlation is achieved demonstrating high confidence in the MATLAB code [64].

Table 1. Comparison of skin friction $f''(0)$ with Yousef et al. [37] and Mahmoud [58] for various values of α_1 when $\alpha_2 = M = \lambda = S_1 = 0$ and $\beta \to \infty$ (Newtonian case).

α_1	*Mahmoud et al. [58]*	*Yousef et al. [37]*	Present results (Bvp4c)
0.0	1.00140	1.00139983	1.0000
1.0	1.41424	1.41422875	1.4142
3.0	2.00000	2.000000	2.0000
5.0	2.44950	2.44948791	2.4494

Table 1 also shows that skin friction is enhanced with increasing Darcy parameter (α_1).

5.RESULTS AND DISCUSSION

In this section, detailed graphical solutions are presented in **Figs. 2-12** for the influence of all key control parameters on velocity, temperature and concentration fields. Additionally, **Tables 2 and 3** provide the solutions for Nusselt and Sherwood numbers.

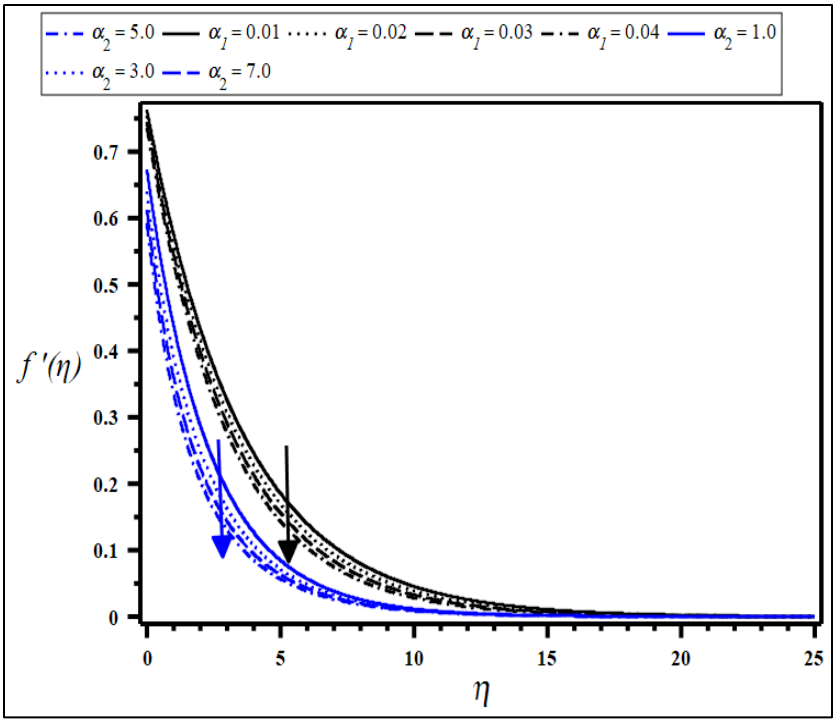

Fig. 2. Variation of velocity $f'(\eta)$ with α_1 & α_2 .

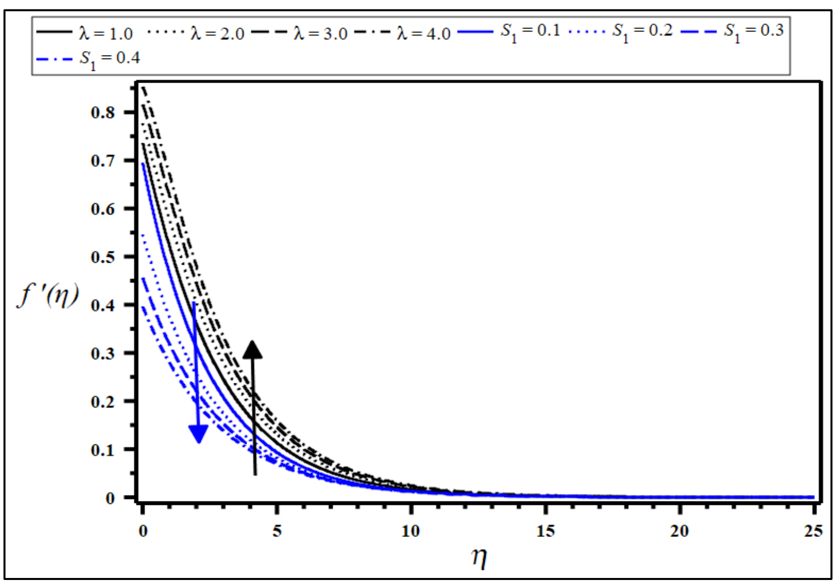

Fig. 3. Variation of velocity $f'(\eta)$ with λ & S_1.

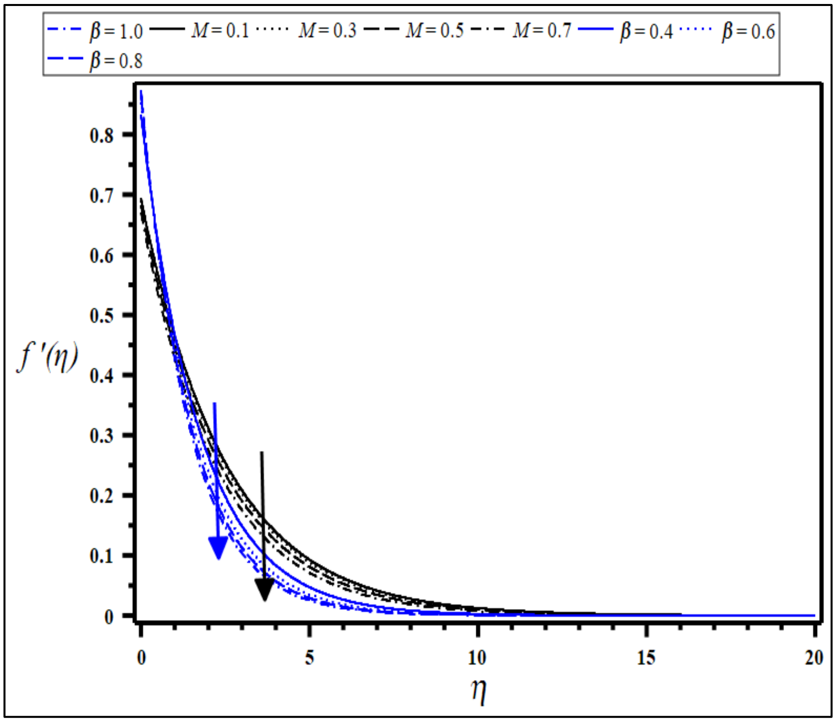

Fig. 4. Variation of velocity $f'(\eta)$ with M & β.

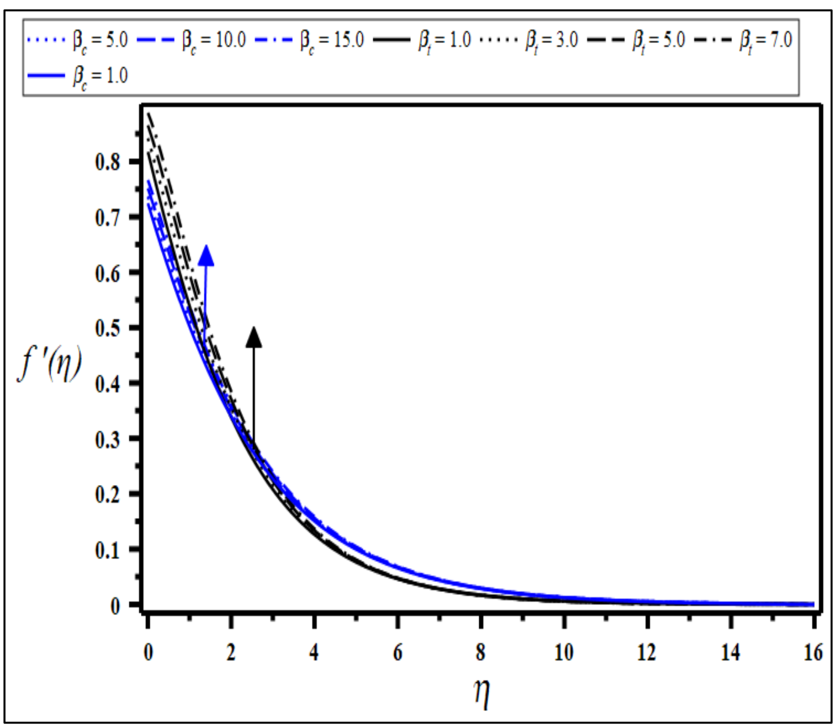

Fig. 5. Variation of velocity $f'(\eta)$ with β_t & β_c .

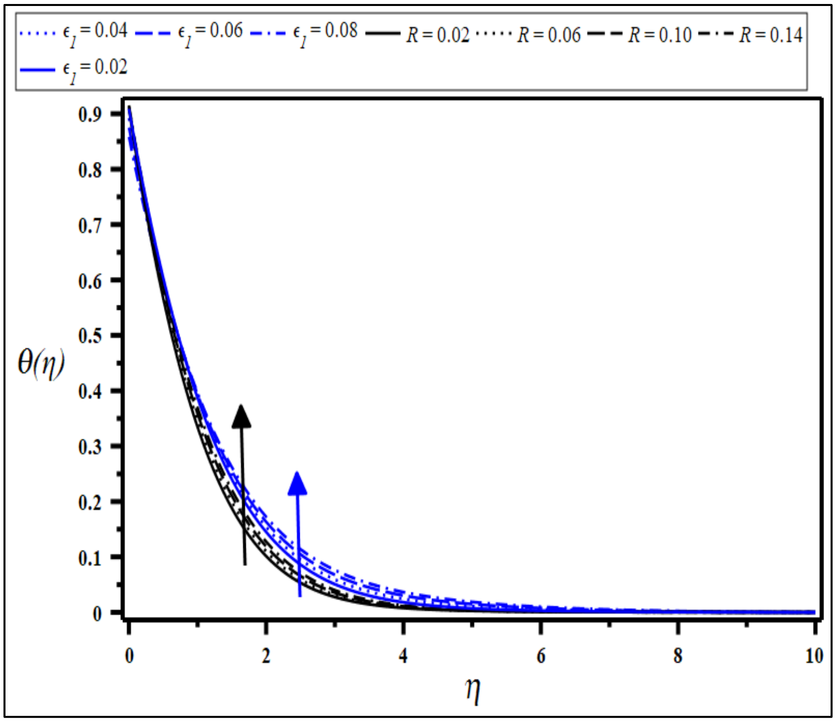

Fig. 6. Variation of temperature $\theta(\eta)$ with R & ε_1.

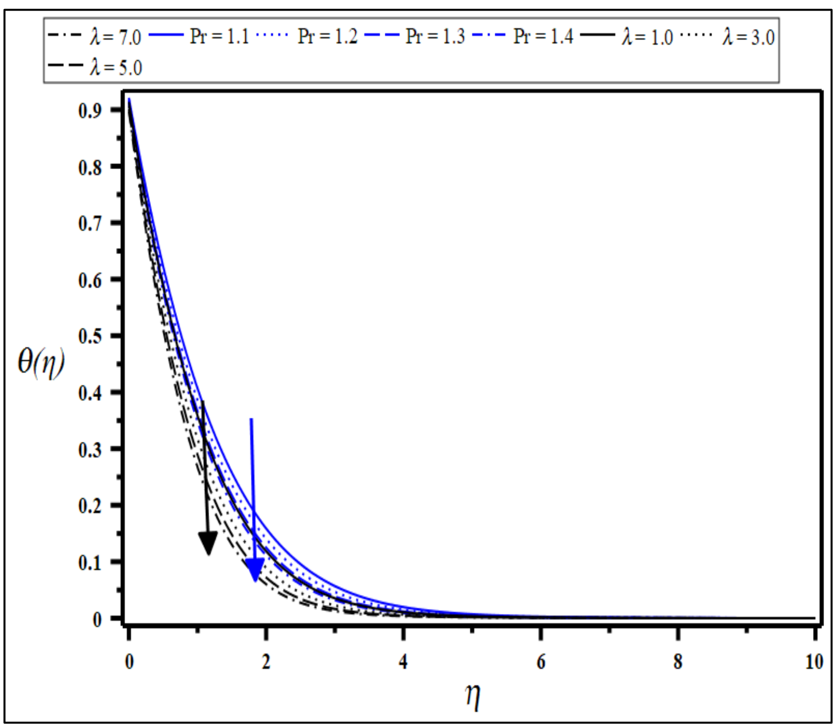

Fig. 7. Variation of temperature $\theta(\eta)$ with $\Pr$ & λ.

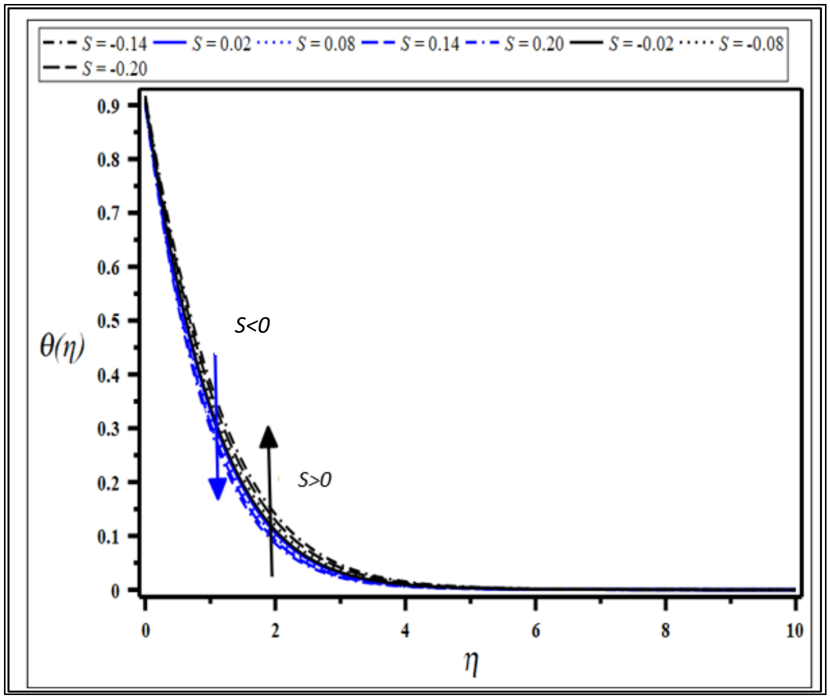

Fig. 8. Variation of temperature $\theta(\eta)$ with *S*.

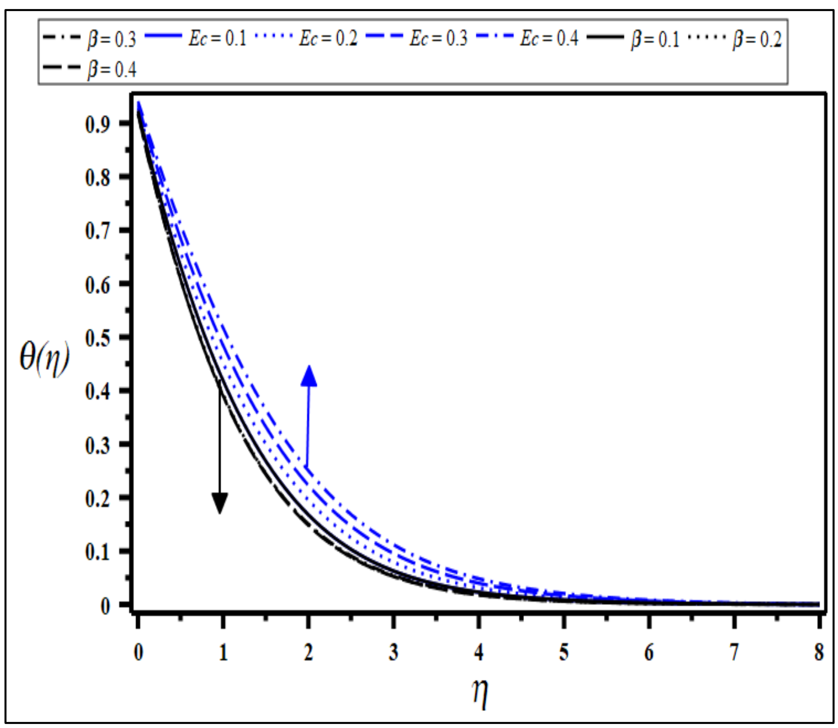

Fig. 9. Variation of temperature $\theta(\eta)$ with Ec & β.

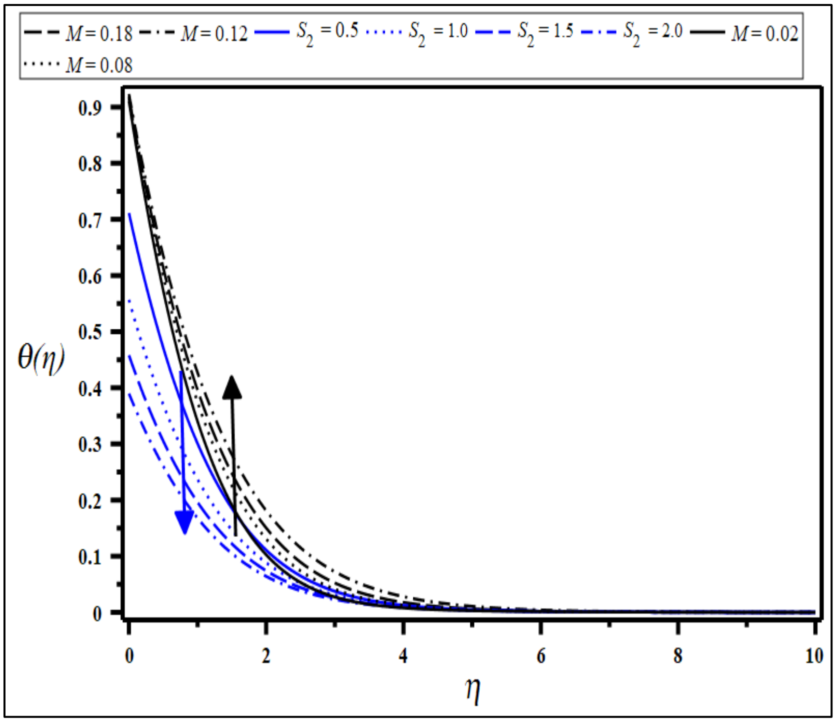

Fig. 10. Variation of temperature $\theta(\eta)$ with S_2 & M .

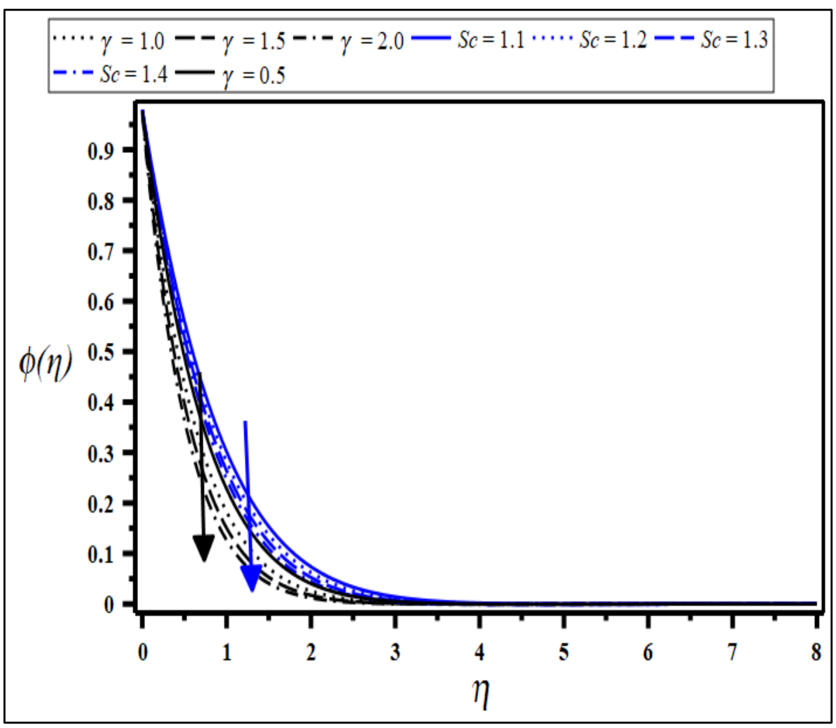

Fig. 11. Variation of concentration $\phi(\eta)$ with Sc & γ .

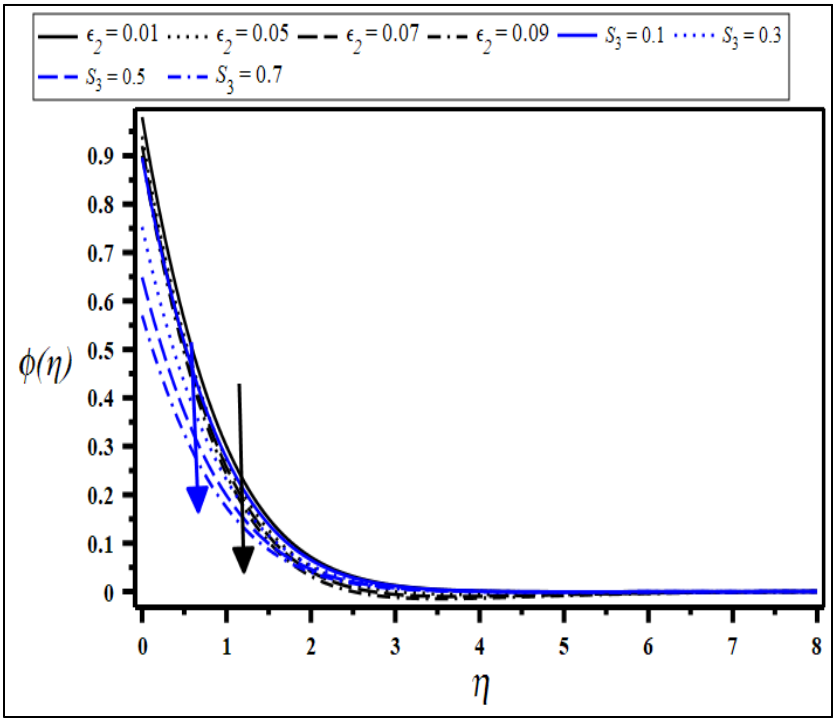

Fig. 12. Variation of concentration $\phi(\eta)$ with ε_2 & S_3.

Table 2. Numerical values of local Nusselt numbers $Nu_x \mathrm{Re}_x^{\frac{1}{2}} = -\left(1+\frac{4}{3}R\right)\theta'(0)$ for the effect of different physical parameters.

R	β	ε_1	S_2	M	λ	Numerical (Bvp4c)
0.5	0.1	0.01	0.01	0.1	0.1	0.4024
1.0						0.2352
1.5						0.1563
0.5	0.3					0.4186
	0.7					0.4087
	0.9					0.4043
	0.1	0.02				0.4021
		0.03				0.4014
		0.04				0.4005
		0.01	0.03			0.3972
			0.07			0.3871
			0.09			0.3821
			0.01	0.5		0.3912
				1.0		0.3591
				1.5		0.3142

				0.1	0.3	0.4094
					0.7	0.4217
					0.9	0.4273

Table 3. Numerical values of Sherwood numbers $Sh_x \mathrm{Re}_x^{-\frac{1}{2}} = -\phi'(0)$ for the effect of different physical parameters.

Sc	ε_2	γ	S_3	Numerical (Bvp4c)
1.1	0.01	0.1	0.01	1.0395
1.3				1.1368
1.5				1.2267
1.1	0.02			1.2228
	0.03			1.2191
	0.04			1.2152
	0.01	0.5		1.2296
		1.0		1.4293
		1.5		1.6017
		0.1	0.2	0.9978
			0.3	0.9784
			0.4	0.9593

5.1 Impact of α_1 and α_2 on velocity field:

The influence of Darcian parameter, α_1 and Forchheimer inertial coefficient parameter α_2 on velocity distribution for fixed values of other pertinent variables is visualized in **Fig. 2.** For fixed porosity Φ (as considered here), this parameter is inversely proportional to permeability, K^*. It features in the term, $-\alpha_1\left(1+\frac{1}{\beta}\right)f'$ in the dimensionless hydrodynamic boundary layer Eqn. (10). As this parameter increases the Darcian bulk matrix drag is elevated since the permeability is reduced. Less space is available to the magnetic polymer to percolate via the porous medium and this induces strong deceleration in the flow i. e. a reduction in velocity. Asymptotically smooth decays in the velocity profiles are computed in the free stream, confirming the prescription of an adequately large infinity boundary condition in the MATLAB computations. Momentum boundary layer thickness is therefore enhanced in the coating regime. A strong retardation is also induced in the flow with elevation in Forchheimer parameter, which also features in the second-degree velocity term, $-\alpha_2 f^{'2}$ in eqn. (10). Although associated with greater inertial effects in the percolating magnetic polymer, the net effect is to impede the flow. The second order drag therefore also inhibits momentum diffusion and boosts the hydrodynamic boundary layer thickness. It is also noteworthy that despite substantial deceleration in the flow, negative velocities are never computed. In other words, the porous medium successfully damps the extruding boundary layer flow, allowing for a more controlled production of the coating [2, 65], but does not induce flow reversal or separation.

5.2 Impact of λ and S_1 on velocity field:

Fig. 3 depicts influence of velocity (momentum) slip parameter S_1 and mixed convection parameter λ. It is evident that there is inverse relationship between mixed convection parameter λ and velocity slip parameter S_1. We noticed that the escalating values of velocity slip parameter S_1 induce a strong decline in velocity i. e. flow deceleration. The slip effect at the wall induces a delay in momentum transfer, as noted in [39]; this curtails the boundary layer development and produces deceleration and a thicker momentum boundary layer. The implication is that when slip is ignored in mathematical models i. e. in the boundary condition (13), $f^{'}(0) = 1 + S_1\left(1 + \frac{1}{\beta}\right) f^{''}(0)$ $\rightarrow 0$ *as* $S_1 \rightarrow 0$, then the velocity distribution is *over-predicted* which negatively impacts on ability of designers to control other properties in the coating [2] including thermal and species distribution characteristics. The inclusion of wall momentum slip is therefore strongly advised in modern magnetic polymer coating analysis and design. Conversely the boost in mixed convection parameter $\lambda\,(= 1,2,3,4)$ increases. This is due to the fact that with the growth in mixed convection parameter, the contribution of *stronger thermal convection currents* enhances momentum transfer. The term, $+\lambda[(1 + \beta_t\theta)\theta]$ in eqn. (10) which couples the momentum field to the energy field (eqn. 11) is therefore amplified and this leads to an acceleration in the flow and a thinner hydrodynamic boundary layer. In both sets of profiles, the strongest modifications in velocity are observed at the wall (sheet) and progressively the effects are diminished as we proceed into the boundary layer transverse to the wall. Again, convergence of profiles is always achieved comfortably in the free stream (edge of the boundary layer) as testified to by the asymptotically smooth decays at large values of transverse coordinate, further confirming that sufficiently large infinity boundary condition values are specified in the MATLAB code.

5.3 Impact of M and β on velocity field:

Fig. 4 depicts the impacts of magnetic interaction number M and Casson rheological parameter β on velocity $f'(\eta)$. It is evident that a hike in M values from 0.1 (weak magnetic field) to 0.7 (stronger magnetic field) decreases the velocity $f'(\eta)$. The parameter M arises only in the Lorentzian drag term, $-M^2 f'$ in the momentum eqn. (10). Although linear this term has a dramatic influence on the flow. *M* defines the relative influence of electromagnetic to inertial forces in the regime. It is in fact known as the *Stuart magnetic interaction number* and is equivalent to the ratio of the square of the Hartmann magnetic number to the Reynolds number. It therefore does not feature viscous force explicitly but does enable the impact of external magnetic field intensity to be assessed relative to the inertial force in the regime. The impeding nature of the electromagnetic force decelerates the flow but does not induce backflow as positive values are always computed. Hydrodynamic boundary layer thicknesses is therefore increased with stronger external magnetic field. The advantage of this mechanism is that it is non-intrusive unlike the porous medium. The magnetic polymer characteristics can be adjusted easily via even a uniform magnetic field as confirmed in Kronmüller and Parkin [65]. Velocity $f'(\eta)$ is also strongly reduced with an increment in Casson non-Newtonian parameter, β. The Casson fluid parameter β is directly proportional to the viscosity of the polymer. Higher values of β therefore produce a greater viscosity in the polymer which enhances the resistance to flow. The term, $-\alpha_1\left(1+\frac{1}{\beta}\right)f'$ in the momentum boundary layer eqn. (10) is therefore adjusted and this strongly modifies the momentum transfer. A thicker velocity boundary layer is produced.

5.4 Impact of β_t and β_c on velocity field:

Fig. 5 illustrates the evolution in velocity profile $f'(\eta)$ with the nonlinear thermal convection parameter (β_t) and nonlinear concentration convection parameter (β_c). As the nonlinear thermal convection parameter $(\beta_t = 1.0, 3.0, 5.0, 7.0)$ increases, the impact on the velocity field $f'(\eta)$ becomes more pronounced. Higher values of this parameter (β_t) imply that the temperature difference has a more significant influence on the buoyancy forces. Consequently, the fluid motion becomes more vigorous and the velocity field $f'(\eta)$ exhibits stronger convective patterns. The fluid flow tends to develop larger and more coherent structures, characterized by stronger vortices and flow acceleration in the boundary layer. Similarly, in the context of nonlinear concentration convection parameter (β_c), this parameter represents the nonlinearity in the relationship between concentration gradients and the driving forces. As the nonlinear concentration convection parameter $(\beta_c = 1.0, 5.0, 10.0, 15.0)$ increases, the velocity field $f'(\eta)$ is increasingly affected. Higher values of this parameter (β_c) imply that the concentration gradients have a more substantial influence on the momentum transfer. Consequently, the fluid flow becomes more intense and the velocity field $f'(\eta)$ exhibits stronger convective behavior. The fluid motion develops more complex patterns with enhanced mixing and transport characteristics. Both nonlinear convection parameters feature in the complex term, $+\lambda[(1+\beta_t\theta)\theta + N(1+\beta_c\phi)\phi]$ *in the hydrodynamic boundary layer eqn. (10). The proportionality is clearly linear and a strong modification in velocity will be generated with a change in both nonlinear convective parameters*. However, the modifications in velocity are more pronounced near the wall for β_t and further into the boundary layer for β_c

5.5 Impact of R and ε_1 on temperature field:

Fig. 6 depicts the influence of the radiation parameter, R and the thermal stratification parameter ε_1 on temperature profiles in the boundary layer. Evidently there is a strong temperature enhancement with increment in R and also the thermal stratification parameter ε_1. The thermal conduction term $\left(1+\frac{4}{3}R\right)\theta''$ in the energy eqn. (11) is modified by the presence of thermal radiation. $R = \frac{4\sigma^* T_\infty^3}{kk^*}$ and this parameter is also known as the Stark number or Rosseland-Boltzmann number. It embodies the relative contribution of radiation heat transfer to conduction heat transfer. When *R = 1* both modes contribute equally. When radiation is absent, $R = 0$. When R < 1, thermal conduction dominates thermal radiation. When $R > 0$, radiative flux is dominant over conductive heat transfer, and this energizes the boundary layer and encourages thermal diffusion. Temperatures are therefore elevated as is thermal boundary layer thickness. The Rosseland diffusion model while limited to optically thick magnetic polymers, does provide a good approximation for boundary layer flows and correctly predicts an elevation in temperature. It is noteworthy that neglection of a radiative flux model in the formulation will lead to under-prediction in temperatures. Since many magnetic polymers are synthesized at high temperature, this can lead to erroneous results for designers. Therefore, it is important to include a suitable radiative flux model in simulations. Of course, there is a hierarchy of complexity involved in radiative heat transfer simulations. Optical thickness variation, non-gray and scattering effects where radiation is attenuated cannot be accommodated by the Rosseland flux model. Other more sophisticated models are required such as the two-flux Schuster-Schwartzchild model or the Cogley-Vincenti-Giles model. These have not been considered here but do constitute good pathways for refining the radiative modelling aspect of the present work and are under consideration for future investigations. The significant boost in temperature with thermal stratification is associated with enhanced thermal diffusion in the boundary layer. When stratification is present, heat is convected more efficiently through the sub-layers of the boundary layer. Molecular conduction is also amplified, and thermal boundary layer thickness is enhanced. Ignoring stratification i. e. vanishing ε_1 therefore also leads to an under-prediction in temperatures in the magnetic polymer.

5.6 Impact of Pr and λ on temperature field:

Fig. 7 display the influence of the mixed convection parameter λ and the Prandtl number $\Pr$ on the temperature profiles. Prandtl number expresses the ratio of momentum diffusivity to thermal diffusivity. It is also inversely proportional to the thermal conductivity of the magnetic polymer. Higher Prandtl number therefore implies a lower thermal conductivity. Increment in Prandtl number therefore suppresses temperatures in the boundary layer and reduces thermal boundary layer thickness. In order to control the rate of cooling at the wall, the Prandtl number can be used as a controlling factor in magnetic polymer manufacture. Heat has a tendency to diffuse quickly from the walls for smaller $\Pr$ values. A regression in the temperature and the thermal boundary layer thickness is also computed with an enhancement in mixed convection parameter λ. Physically speaking there is an increase in thermal buoyancy force with larger mixed convection parameter. The amplification in natural convection currents assists momentum diffusion but inhibits thermal diffusion. This results in a diminishing in heat transmission and a strong cooling in the boundary layer. Thermal boundary layer thickness is therefore also depleted.

5.7 Impact of S ($S>0$ and $S<0$) on temperature field:

The effect of heat source $(S>0)$ and heat sink $(S<0)$ on the temperature profile $\theta(\eta)$ is portrayed in **Fig. 8**. Increased heat source i. e. volumetric heat generation $(S>0)$ values which correspond to a hot spot on the substrate cause an increase in the temperature and a boost in thermal boundary layer thickness. The converse response is computed for heat sink $(S < 0)$ which corresponds to absorption of thermal energy via for example a drain in the substrate. Thermal boundary layer is reduced with stronger heat sink and a strong cooling effect is produced in the coating.

5.8 Impact of Ec and β on temperature field:

In **Fig. 9**, the effects of Eckert number Ec and Casson parameter β on temperature field $\theta(\eta)$ are displayed. A significant increase in the temperature is observed as Ec increases. It is apparent that temperature is enhanced significantly with increasing values of Eckert number. This parameter arises in the viscous heating term, $+\boldsymbol{Pr}\,E\,c\left(1+\frac{1}{\beta}\right)f''^{2}$ and Ohmic heating (Joule dissipation) term, $+\boldsymbol{Pr}\,E\,cM^{2}f'^{2}$ in the energy eqn. (11). The first term represents the kinetic energy dissipated due to internal friction in the magnetic polymer. The second term is associated with heat generation against the magnetic field action. Both terms exert a marked influence on thermal diffusion. Clearly the neglection of viscous heating ($Ec = 0$) in mathematical models leads to an under-prediction in temperatures i. e. cooling is observed in simulations, not heating. This leads to difficulty in optimizing the constitution of the magnetic polymer [65]. Dissipation effects are real in polymers and must be included in robust analysis of their behaviour [2, 28, 30]. With greater Casson parameter β i. e. increment through $\beta = 0.1, 0.2, 0.3, 0.4$ there is a strong decline in the temperature $\theta(\eta)$ and related thermal boundary layer thickness on the stretching sheet surface. Although not arising explicitly in the energy eqn. (11), the Casson rheological parameter exerts an indirect effect via the many coupling terms between the velocity and temperature fields, for example the nonlinear convective terms, $\boldsymbol{Pr}\,f\,\theta' - \boldsymbol{Pr}\,f'\,\theta$ *in the energy eqn. (11) and the terms* $+\lambda[(1+\beta_t\theta)\theta + N(1+\beta_c\phi)\phi]$ *in the momentum eqn. (10).* The modification in viscosity of the polymer with variation in β clearly influences the temperature distribution strongly.

5.9 Impact of S_2 and M on temperature field:

The effects of thermal slip parameter S_2 and magnetic interaction parameter M on temperature field are computed in **Fig. 10**. There is a a significant boost in temperatures associated with stronger electromagnetic force i. e. higher M values. The magnetic polymer has to exert supplementary work in dragging itself against the action of the Lorentzian magnetic body force.

This kinetic energy is dissipated as heat and is also intimately connected to the Ohmic dissipation effect. The influence due to magnetic field is however not indirect, it is largely associated with the Ohmic dissipation effect as computed in the term, $+\boldsymbol{Pr}\, E\, cM^2 f'^2$ in the energy eqn. (11). Although a hydrodynamic effect, the electromagnetic Lorentz force therefore exerts a non-trivial influence on temperature distribution which is important again in thermal management of the coating processes involved in magnetic polymer manufacturing systems. Thermal boundary layer thickness is therefore also enhanced with stronger magnetic field. Temperature field $\theta(\eta)$ is however reduced with greater thermal slip parameter S_2. This parameter arises as with the momentum slip parameter in the associated boundary condition at the wall i. e. $\theta(0) = 1 - \epsilon_1 + S_2\theta'(0)$ in eqn. (13). There is a considerable decrease in temperature $\theta(\eta)$ in particular in the vicinity of the wall; this effect progressively diminishes further into the boundary layer. Thermal slip produces a jump effect in the conduction at the wall. The convective motion is inhibited by this suppression in thermal conduction and thermal diffusion is decreased. This reduces thermal boundary layer thickness strongly and induces a significant cooling effect in the boundary layer.

5.10 Impact of Sc and γ on concentration field:

Fig. 11 visualizes the response in species concentration distribution with a change in Schmidt number Sc and chemical reaction parameter γ. There is a consistent strong decline in the concentration of the reactant when Sc and γ are increased. Species boundary layer thicknesses are therefore depleted with stronger chemical reaction rate and higher Schmidt number. After a critical value of transverse coordinate, η, the concentration profiles become constant, indicating that the concentration of the reactant remains unchanged with Sc and γ. The modifications in concentration magnitudes are therefore confined to the near-wall zone. Schmidt number represents the ratio of momentum to species (molecular) diffusivity in the boundary layer. When Sc = 1 both momentum and concentration boundary layer thickness are equal. For $Sc > 1$ the momentum diffusion rate dominates the species diffusion rate and vice versa for $Sc < 1$. The computations correspond to for example oxygen diffusing in magnetic polymer [65] which assists in homogenizing the constitution of the polymer coating. The boost in chemical reaction parameter corresponds to a more intense homogenous first order destructive reaction as embodied in the negative term, $-Sc\gamma\phi$ in the concentration boundary layer eqn. (12). This physically implies that more of the original reactant e. g. oxygen, is converted into a new species and therefore logically the original concentration of species will be suppressed as observed in Fig. 11. Since chemical reactions are critical in inducing morphological changes in magnetic polymers, the inclusion of a reactive term in the species eqn. (12) is important.

5.11 Impact of ε_2 and S_3 on concentration field:

Fig. 12 clarify the variations of concentration with variation in solutal stratification parameter ε_2 and solutal slip parameter S_3. It is evident that an intensification in solutal slip parameter and solutal stratification parameter both manifest in a significant depletion in species concentration and species boundary layer thickness. Whereas thermal stratification enhances temperatures (as described earlier), solutal stratification has the opposite effect. The associated term in eqn. (12), $-Sc\varepsilon_2 f^{'}$ inhibits species diffusion strongly. Molecular motion of the species is different from thermal diffusion. The concentration distribution $\phi(\eta)$ is also suppressed with greater solutal slip parameter. This parameter arises in the augmented wall boundary condition, $\phi(0) = 1 - \epsilon_2 + S_3\phi^{'}(0)$ in eqn. (13). The inhibition in molecular motion is substantial especially near the wall and this reduces mass transfer into the boundary layer leading to a reduction in concentration boundary layer thickness.

5.12 Impact of selected parameters on local Nusselt number

Table 2 shows the response in local Nusselt number, $Nu_x \mathrm{Re}_x^{\frac{1}{2}} = -\left(1+\frac{4}{3}R\right)\theta'(0)$ to variation in selected parameters. Increasing radiative parameter, *R* produces a strong decrement in Nusselt number since heating due to thermal radiative flux within the boundary layer draws thermal energy away from the stretching sheet. This reduces the heat transmission to the wall and therefore Nusselt numbers plummet. With increasing Casson non-Newtonian parameter, β, Nusselt number is also reduces. Again, this is associated with the heating within the boundary layer and the associated reduction in thermal energy transferred to the wall out of the boundary layer. Increment in both thermal stratification parameter ε_1 and solutal slip parameter S_2 generally suppresses the Nusselt number, which also implies that thermal convection relative to thermal conduction at the stretching sheet is reduced. With greater magnetic number, *M* the Nusselt number is also depleted whereas with increased mixed convection parameter λ it is enhanced (since in this case the boundary layer is cooled implying heat is effectively transmitted towards the wall).

5.13 Impact of selected parameters on Sherwood number

Table 3 shows the response in local Sherwood numbers $Sh_x \mathrm{Re}_x^{-\frac{1}{2}} = -\phi'(0)$ with selected control parameters. An elevation in Schmidt number and chemical reaction parameter are observed to both boost the Sherwood number i.e. enhance mass transfer of the species to the boundary. The contrary response is computed for increasing solutal stratification parameter ε_2 and solutal slip parameter S_3. Larger Sherwood numbers imply the net mass transfer is to the wall. The concentration within the boundary layer is therefore depleted. The trends are therefore consistent with the earlier computations for concentration distribution given in **Figs. 11 and 12**.

6.CONCLUSIONS

A theoretical and computational study of *thermo-solutal magnetohydrodynamic (MHD) dissipative non-Newtonian Casson viscoplastic coating boundary layer flow of a stretching substrate adjacent to a porous medium, considering the influence of chemical reactions and thermal radiation subject to a transverse static magnetic field*. *This is the novelty and focus of the present article which motivated by magnetic polymer manufacturing applications, explores the combined effects of Darcy and Forchheimer drag forces, radiative flux (via the Rosseland model), hydrodynamic, thermal and concentration slip, heat source/sink [59, 60] and dual thermal/solutal stratification effects [61-63] on transport characteristics. Additionally viscous dissipation and Ohmic heating (Joule dissipation) are included*. Robust scaling similarity variables are deployed to transform the governing partial differential equations into ordinary differential equations. Subsequently, the emerging dimensionless coupled nonlinear boundary value problem is solved utilizing the Bvp4c method in MATLAB version 2022. Validation with previous studies ignoring porous media drag force, magnetic field, mixed convection and momentum wall slip effects has been included. The computations have shown that:

(i) An increase in Schmidt number and chemical reaction parameter both reduce species concentrations but boost the Sherwood number.

(ii) An elevation in solutal stratification parameter ε_2 and solutal slip parameter S_3 both reduce concentrations but enhance the Sherwood number.

(iii) Increased heat source i. e. volumetric heat generation $(S > 0)$ increases temperature and thermal boundary layer thickness whereas increased $(S < 0)$ generates the converse effect.

(iv) Increasing radiative parameter, *R*, Casson non-Newtonian parameter, β, Nusselt number, thermal stratification parameter ε_1, solutal slip parameter S_2 and magnetic number, *M* generally reduce the Nusselt number.

(v) Increasing mixed convection parameter produces strong cooling in the boundary layer and elevates the Nusselt number.

(vi) Temperature and thermal boundary thickness is boosted strongly with increasing values of Eckert number due to the associated effects of viscous dissipation and Ohmic heating (Joule dissipation).

(vii) Temperature and thermal boundary layer thickness are reduced with increment in Casson parameter β.

(viii) Velocity $f'(\eta)$ is reduced with greater Darcian parameter, α_1 , Forchheimer parameter α_2 , magnetic interaction parameter, M , Casson rheological parameter β and momentum slip parameter S_1, whereas flow acceleration is induced with increasing mixed convection parameter.

The present study has revealed some interesting features of electro-conductive polymer thermal processing with multiple effects. However magnetic induction [65] and ferromagnetic [66] effects have been neglected. These are also important in modern magnetic polymer manufacturing and will be addressed in the near future.

REFERENCES

[1] Bird, R B, Armstrong, R C, and Hassager, O. *Dynamics of Polymeric Liquids. Vol. 1, Fluid Mechanics*. John Wiley, New York, USA (1987)

[2] V. S. Kathavate and P. P. Deshpande, *Smart Coatings: Fundamentals, Developments and Applications*, CRC Press, Florida, USA (2023).

[3] Xiao Kuang *et al.,* Magnetic dynamic polymers for modular assembling and reconfigurable morphing architectures *Adv. Mater.* 2021, 2102113 (12 pages).

[4] B. Nagarajan, Development and characterization of field structured magnetic composites, *Polymers (Basel).* 2021 Sep; 13(17): 2843.

[5] Volpe V., D'Auria M., Sorrentino L., Davino D., Pantani R. Injection molding of magneto-sensitive polymer composites. *Mater. Today Commun.* 2018;15: 280–287.

[6] Nagarajan B., Kamkar M., Schoen M.A.W., Sundararaj U., Trudel S., Qureshi A.J., Mertiny P. Development and characterization of stable polymer formulations for manufacturing magnetic composites. *J. Manuf. Mater. Process.* 2020; 4:4.

[7] Awais, M., Ehsan Awan, S., Asif Zahoor Raja, M., Parveen, N., Khan, W. U., Yousaf Malik, M., & He, Y. (2021). Effects of variable transport properties on heat and mass transfer in MHD bioconvective nanofluid rheology with gyrotactic microorganisms: Numerical approach. *Coatings*, *11*(2), 231

[8] Awais, M., Kumam, P., Ali, A., Shah, Z., & Alrabaiah, H. (2021). Impact of activation energy on hyperbolic tangent nanofluid with mixed convection rheology and entropy optimization. *Alexandria Engineering Journal*, *60*(1), 1123-1135.

[9] Nasir, M., Waqas, M., Bég, O. A., Basha, D. B., Zamri, N., Leonard, H. J., & Khan, I. (2022). Chemically reactive Maxwell nanoliquid flow by a stretching surface in the frames of Newtonian heating, nonlinear convection and radiative flux: Nanopolymer flow processing simulation. *Nanotechnology Reviews*, *11*(1), 1291-1306.

[10] A. Shahid, M. M. Bhatti, O. Anwar Bég and A. Kadir, Numerical study of radiative Maxwell viscoelastic magnetized flow from a stretching permeable sheet with the Cattaneo–Christov heat flux model, *Neural Computing and Applications*, 30, 3467–3478 (2018).

[11] Awais, M., Ehsan Awan, S., Raja, M. A. Z., Nawaz, M., Khan, W. U., Yousaf Malik, M., & He, Y. (2021). Heat transfer in nanomaterial suspension (CuO and Al2O3) using KKL model. *Coatings*, *11*(4), 417.

[12] Anjum, N., Khan, W. A., Azam, M., Ali, M., Waqas, M., & Hussain, I. (2022). Significance of bioconvection analysis for thermally stratified 3D Cross nanofluid flow with gyrotactic

microorganisms and activation energy aspects. *Thermal Science and Engineering Progress,* 101596.

[13] Awais, M., Rehman, H., Raja, M. A. Z., Awan, S. E., Ali, A., Shoaib, M., & Malik, M. Y. (2022). Hall effect on MHD Jeffrey fluid flow with Cattaneo–Christov heat flux model: An application of stochastic neural computing. *Complex & Intelligent Systems, 8*(6), 5177-5201.

[14] Casson, N. (1959) A flow equation for pigment-oil suspensions of the printing ink type. *In: Mill, C.C., Ed., Rheology of Disperse Systems, Pergamon Press, Oxford,* 84-104.

[15] Alhadhrami, A., Vishalakshi, C. S., Prasanna, B. M., Sreenivasa, B. R., Alzahrani, H. A., Gowda, R. P., & Kumar, R. N. (2021). Numerical simulation of local thermal non-equilibrium effects on the flow and heat transfer of non-Newtonian Casson fluid in porous media. *Case Studies in Thermal Engineering*, *28*, 101483.

[16] Akhtar, S., Almutairi, S., & Nadeem, S. (2022). Impact of heat and mass transfer on the Peristaltic flow of non-Newtonian Casson fluid inside an elliptic conduit: Exact solutions through novel technique. *Chinese Journal of Physics*, *78*, 194-206.

[17] Samrat, S. P., Gangadharaiah, Y. H., Ashwinkumar, G. P., & Sandeep, N. (2022). Effect of exponential heat source on parabolic flow of three different non-Newtonian fluids. *Proceedings of the Institution of Mechanical Engineers, Part E: Journal of Process Mechanical Engineering*, 09544089221083468.

[18] N. S. Akbar, D. Tripathi, O. Anwar Bég, Z. H. Khan, MHD dissipative flow and heat transfer of Casson fluids due to metachronal wave propulsion of beating cilia with thermal and velocity slip effects under an oblique magnetic field, *Acta Astronautica,* 128, 1-12 (2016).

[19] Awais, M., Raja, M. A. Z., Awan, S. E., Shoaib, M., & Ali, H. M. (2021). Heat and mass transfer phenomenon for the dynamics of Casson fluid through porous medium over shrinking wall subject to Lorentz force and heat source/sink. *Alexandria Engineering Journal*, *60*(1), 1355-1363.

[20] B. Vasu, Atul Kumar Ray, O. Anwar Bég and Rama Subba Reddy Gorla, Magneto-bioconvection flow of a Casson thin film with nanoparticles over an unsteady stretching sheet: HAM and GDQ computation, *Int. J. Numerical Methods Heat Fluid Flow,* 29 (11) 4277-4309 (2019).

[21] J. Prakash, D. Tripathi, O. Anwar Bég, V. Srivastava, EMHD Casson hybrid nanofluid flow over an exponentially accelerated rotating porous surface, *J. Porous Media*, 25(4):1–24 (2022).

[22] A. Shahidi, W. Wei, M. M. Bhatti, O. Anwar Bég and Tasveer A. Bég, Mixed convection Casson polymeric flow from a nonlinear stretching surface with radiative flux and non-Fourier thermal relaxation effects: Computation with CSNIS, *ZAMM* (2023). DOI: 10.1002/zamm.202200519 (15 pages)

[23] J. Zueco, O. Anwar Bég, Takhar H. S. & V.R. Prasad, Thermophoretic hydromagnetic dissipative heat and mass transfer with lateral mass flux, heat source, Ohmic heating and thermal conductivity effects: network simulation numerical study, *Applied Thermal Engineering*, 29, 2808-2815 (2009).

[24] Kausar, M. S., Al-Sharifi, H. A. M., Hussanan, A., & Mamat, M. (2022). The Effects of Thermal Radiation and Viscous Dissipation on the Stagnation Point Flow of a Micropolar Fluid over a Permeable Stretching Sheet in the Presence of Porous Dissipation. *Journal of Fluid Dynamics & Materials Processing*, 19(1), 61-81.

[25] T. Thumma, O. Anwar Bég and A. Kadir, Numerical study of heat source/sink effects on dissipative magnetic nanofluid flow from a non-linear inclined stretching/shrinking sheet, *J. Molecular Liquids,* 232, 159-173 (2017).

[26] Awais, M., Awan, S. E., Raja, M. A. Z., & Shoaib, M. (2021). Effects of Gyro-Tactic organisms in bio-convective nanomaterial with heat immersion, stratification, and viscous dissipation. *Arabian Journal for Science and Engineering*, *46*, 5907-5920.

[27] Awais, M., Bibi, M., Ali, A., Malik, M. Y., Nisar, K. S., & Jamshed, W. (2022). Numerical analysis of MHD axisymmetric rotating Bodewadt rheology under viscous dissipation and ohmic heating effects. *Scientific Reports*, *12*(1), 1-17. (variable viscosity model)

[28] M. Kumar, G. J. Reddy, N. N. Kumar *and* O. Anwar Bég, Computational study of unsteady couple stress magnetic nanofluid flow from a stretching sheet with Ohmic dissipation, *Proc. IMechE-Part N: J Nanoengineering, Nanomaterials and Nano-systems* (2019). (15 pages) DOI: 10.1177/2397791419843730

[29] Kausar, M. S., Hussanan, A., Waqas, M., & Mamat, M. (2022). Boundary layer flow of micropolar nanofluid towards a permeable stretching sheet in the presence of porous medium with thermal radiation and viscous dissipation. *Chinese Journal of Physics*, *78,* 435-452.

[30] MD. Shamshuddin, S.O. Salawu, O. Anwar Bég, T. A. Bég and Ali Kadir, Computation of reactive mixed convection radiative viscoelastic nanofluid thermo-solutal transport from a

stretching sheet with Joule heating, *International Journal of Modelling and Simulation* (2021). DOI: 10.1080/02286203.2021.2012635 (26 pages).

[31] D. Murugan, Ashis Kumar Roy, R. Ponalagusamy and O. Anwar Bég, Tracer dispersion due to pulsatile Casson fluid flow in a circular tube with chemical reaction modulated by externally applied electromagnetic fields, *Int. J. Applied and Computational Mathematics (2022). 8:221* https://doi.org/10.1007/s40819-022-01412-3 (23 pages)

[32] M. Shamshuddin, S.R. Mishra, O. Anwar Bég and Ali Kadir, Adomian computation of radiative-convective stretching flow of a magnetic non-Newtonian fluid in a porous medium with homogeneous–heterogeneous reactions, *Int. J Modern Physics B, 33 (2) (2020).* (28 pages).

[33] M. Garvandha, V. K. Narla, D. Tripathi and O. Anwar Bég, Modelling the impact of melting and nonlinear radiation on reactive Buongiorno nanofluid boundary layer flow from an inclined stretching cylinder with cross diffusion and curvature effects, *Applications in Nanotechnology, Book chapter, Energy Systems and Nanotechnology", "Advances in Sustainability Science and Technology" Book Series, Springer-Germany Eds. D. Tripathi and S. SHamra, pp.279-306 (2021).*

[34] Reddy, M. V., Pallavarapu, L., & Vajravelu, K. (2021). A comparative study of MHD non-Newtonian fluid flows with the effects of chemical reaction and radiation over a stretching sheet. *Computational Thermal Sciences: An International Journal*, *13*(5).

[35] Shah, S. A. A., Ahammad, N. A., Din, E. M. T. E., Gamaoun, F., Awan, A. U., & Ali, B. (2022). Bio-convection effects on Prandtl hybrid nanofluid flow with chemical reaction and motile microorganism over a stretching sheet. *Nanomaterials*, *12*(13), 2174.

[36] Sudarsana Reddy, P., & Sreedevi, P. (2022). Impact of chemical reaction and double stratification on heat and mass transfer characteristics of nanofluid flow over porous stretching sheet with thermal radiation. *International Journal of Ambient Energy*, *43*(1), 1626-1636.

[37] Yousef, N. S., Megahed, A. M., Ghoneim, N. I., Elsafi, M., & Fares, E. (2022). Chemical reaction impact on MHD dissipative Casson-Williamson nanofluid flow over a slippery stretching sheet through porous medium. *Alexandria Engineering Journal*, *61*(12), 10161-10170.

[38] Nasir, M., Waqas, M., Bég, O. A., Ameen, H. F. M., Zamri, N., Guedri, K., & Eldin, S. M. (2022). Analysis of Nonlinear Convection–Radiation in Chemically Reactive Oldroyd-B Nanoliquid Configured by a Stretching Surface with Robin Conditions: Applications in Nano-Coating Manufacturing. *Micromachines*, *13*(12), 2196

[39] Y. Lou *et al.*, Wall Slip Behaviour of Polymers Based on Molecular Dynamics at the Micro/Nanoscale and Its Effect on Interface Thermal Resistance, *Polymers* 2020, *12*(10), 2182; **https://doi.org/10.3390/polym12102182**

[40] Dawson, A.; Rides, M.; Allen, C.R.G.; Urquhart, J.M. Polymer mould interface heat transfer coefficient measurements for polymer processing. *Polym. Test.* **2008**, *27*, 555–565.

[41] Liu, Y.; Gehde, M. Effects of surface roughness and processing parameters on heat transfer coefficient between polymer and cavity wall during injection molding. *Int. J. Adv. Manuf. Technol.* 2016, *84*, 1325–1333.

[42] Ge, S.; Chen, M. Molecular dynamics simulations of the effect of velocity slip on the solid-liquid interfacial thermal resistance. *J. Eng. Thermophys.* 2013, *34*, 1527–152.

[43] Md Faisal Md Basir, M.J. Uddin, A. I. Md. Ismail and O. Anwar Bég, Unsteady bio-nanofluid slip flow over a stretching cylinder with bioconvection Schmidt and Péclet number effects, *AIP Advances,* 6, 055316-1 - 055316-15 (2016).

[44] Zubair, M., Waqas, M., Nasir, M., Bafakeeh, O. T., Ameen, H. F. M., & Galal, A. M. (2022). A theoretical study on partial slip impact in radiative-hydromagnetic liquid configured by extending surface. *International Journal of Modern Physics B*, 2350074.

[45] M. Shamshuddin, U. S. Khan, O. Anwar Bég, T.A. Bég, Hall current, viscous and Joule heating effects on steady radiative 3-D magneto-power-law polymer dynamics from an exponentially stretching sheet with power-law slip velocity: a numerical study, *Thermal Science and Engineering Progress, 20 (2020) 100732. doi.org/10.1016/j.tsep.2020.100732 (13 pages)*

[46] A SubbaRao, V.R. Prasad, N. Bhaskar Reddy, O. Anwar Bég, Modelling laminar transport phenomena in a Casson rheological fluid from an isothermal sphere with partial slip, *Thermal Science - Int. Scientific Journal, 19 (5) 1507-1519 (2015). doi: 10.2298/ TSCI1208 2 8 098S*

[47] Khan, S. U., Al-Khaled, K., & Bhatti, M. M. (2021). Bioconvection analysis for flow of Oldroyd-B nanofluid configured by a convectively heated surface with partial slip effects. *Surfaces and Interfaces*, *23*, 100982.

[48] Javid, K., Kolsi, L., Al-Khaled, K., Omri, M., Khan, S. U., & Abbasi, A. (2022). Biomimetic propulsion of viscoelastic nanoparticles in a curved pump with curvature and slip effects: blood control bio-medical applications. *Waves in Random and Complex Media*, 1-18.

[49] Wang, F., Ahmad, S., Al Mdallal, Q., Alammari, M., Khan, M. N., & Rehman, A. (2022). Natural bio-convective flow of Maxwell nanofluid over an exponentially stretching surface with slip effect and convective boundary condition. *Scientific Reports*, *12*(1), 1-14.

[50] Raza, A., Ghaffari, A., Khan, S. U., Haq, A. U., Khan, M. I., & Khan, M. R. (2022). Non-singular fractional computations for the radiative heat and mass transfer phenomenon subject to mixed convection and slip boundary effects. *Chaos, Solitons & Fractals*, *155*, 111708.

[51] Rana, P., & Gupta, G. (2022). Heat transfer optimization of Marangoni convective flow of nanofluid over an infinite disk with Stefan blowing and slip effects using Taguchi method. *International Communications in Heat and Mass Transfer*, *130*, 105822.

[52] Madhukesh, J. K., Prasannakumara, B. C., Kumar, R. S. V., Rauf, A., & Shehzad, S. A. (2022). Flow of hydromagnetic micropolar-casson nanofluid over porous disks influenced by cattaneo-christov theory and slip effects. *Journal of Porous Media*, *25*(3).

[53] Krishna, M. V. (2022). Analytical study of chemical reaction, Soret, Hall and ion slip effects on MHD flow past an infinite rotating vertical porous plate. *Waves in Random and Complex Media*, 1-27.

[54] Kausar, M. S., Hussanan, A., Mamat, M., & Ahmad, B. (2019). Boundary layer flow through Darcy–Brinkman porous medium in the presence of slip effects and porous dissipation. *Symmetry*, *11*(5), 659.

[55] Zainal, N. A., Nazar, R., Naganthran, K., & Pop, I. (2022). Slip effects on unsteady mixed convection of hybrid nanofluid flow near the stagnation point. *Applied Mathematics and Mechanics*, *43*(4), 547-556.

[56] M.J. Uddin, O. Anwar Bég and N.S. Amin, Hydromagnetic transport phenomena from a stretching or shrinking nonlinear nanomaterial sheet with Navier slip and convective heating: a model for bio-nano-materials processing, *J. Magnetism Magnetic Materials, 368, 252-261(2014).*

[57] Sajid, T., Jamshed, W., Safdar, R., Hussain, S. M., Shahzad, F., Bilal, M., ... & Pasha, A. A. (2022). Features and aspects of radioactive flow and slippage velocity on rotating two-phase Prandtl nanofluid with zero mass fluxing and convective constraints. *International Communications in Heat and Mass Transfer, 136*, 106180.

[58] Mahmoud, M. A. (2007). Thermal radiation effects on MHD flow of a micropolar fluid over a stretching surface with variable thermal conductivity. *Physica A: Statistical Mechanics and its Applications*, *375*(2), 401-410.

[58] M. J. Uddin, M.N. Kabir, O. Anwar Bég and Y. Alginahi, Chebyshev collocation computation of magneto-bioconvection nanofluid flow over a wedge with multiple slips and magnetic induction, *Proc. IMechE: Part N-Journal of Nanomaterials, Nanoengineering and Nanosystems, 232, 109-122 (2018).*

[59] Waqas, M., Nasir, M., Khan, M. I., Boujelbene, M., Alshammari, S., Chouikhi, N., & Rajeh, T. (2022). Marangoni forced convective thermally developed two-phase dusty flow of fluid with heat source/sink phenomenon. *International Journal of Modern Physics B*, 2350126.

[60] O. Anwar Bég, K. Venkatadri, V.R. Prasad, T. A. Bég, A. Kadir and Henry J. Leonard, Numerical simulation of hydromagnetic Marangoni convection flow in a Darcian porous semiconductor melt enclosure with buoyancy and heat generation effects, *Materials Science and Engineering B: Advanced Functional and Solid-State Materials, 261, (2020) 114722. (23 pages)*

[61] Ahmed, M. F., Zaib, A., Ali, F., Bafakeeh, O. T., Tag-ElDin, E. S. M., Guedri, K., ... & Khan, M. I. (2022). Numerical computation for gyrotactic microorganisms in MHD radiative Eyring–Powell nanomaterial flow by a static/moving wedge with Darcy–Forchheimer relation. *Micromachines*, *13*(10), 1768.

[62] Nasir, M., Waqas, M., Bég, O. Anwar, Zamri, N., Leonard, H. J., & Guedri, K. (2022). Dynamics of tangent-hyperbolic nanoliquids configured by stratified extending surface: Effects of transpiration, Robin conditions and dual stratifications. *International Communications in Heat and Mass Transfer*, *139*, 106372.

[63] Nasir, M., Waqas, M., Zamri, N., Jameel, M., Guedri, K., & Galal, A. M. (2022). Rheology of tangent-hyperbolic (TH) nanoliquid configured by stretchable stratified surface considering transpiration effects. *International Journal of Modern Physics B*, 2350057.

[64] **https://uk.mathworks.com/products/new_products/latest_features.html** (2022).

[65] Helmut Kronmüller and Stuart Parkin (Editors), *Handbook of Magnetism and Advanced Magnetic Materials*, 5 Volume Set, 3064 Pages, Wiley, New York, USA (2007).

[66] S.O. Solawu, M. Shamshuddin, O. Anwar Bég, Influence of magnetization, variable viscosity and thermal conductivity on Von Karman swirling flow of H_2O-Fe_3O_4 and H_2O-Mn-$ZNFe_2O_4$ ferromagnetic nanofluids from a stretchable rotating disk: smart spin coating simulation, *Materials Science and Engineering B, 279 (2022) 115659 (13 pages).*